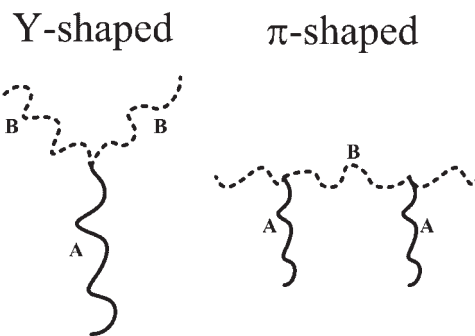


A Comparison of Y-, H-, and π -shaped Diblock Copolymers via Dissipative Particle Dynamics

Ching-I Huang,* Li-Fan Yang, Chih-Hao Lin, Hsu-Tung Yu

The phase behaviors, molecular conformations, and structural length scales of Y- (AB_2), H- (B_2AB_2), and π -shaped $[B(A)B(A)B]$ copolymers are compared using dissipative particle dynamics. Though their phase diagrams are similar, the stability of microstructures is enhanced with increasing complexity of molecular architecture (linear \rightarrow Y \rightarrow H or π). In addition, the greater entropy loss associated with the disorder-to-order transition for H and π architectures makes it more difficult for them to undergo a microphase separation. When the H and π molecules pack to form an ordered structure, due to the significant presence of the chains in a bridge conformation, the structural length scales are strongly restricted.



Introduction

Recently, with the improvement in synthetic techniques, the morphological behavior of copolymers with more complex architectures has been intensively studied. Graft copolymers are one of the molecular architectures that have attracted a lot of attention. For example, miktoarm star, H-shaped, and π -shaped diblock copolymers are the special graft copolymers. So far, the resulting phase behavior of simple A_mB_n miktoarm star copolymers has been well understood from both experimental and theoretical points of view.^[1–12] Though there exist a few experimental morphological studies on the H-shaped and π -shaped diblock copolymers,^[13–21] most of the relevant understanding of their morphological behavior are based on the constituting Y-shaped (i.e., three-miktoarm) copolymers. To our knowledge, no systematic phase behaviors of these H- and π -shaped architectures have been addressed theoretically. In this paper, we therefore

compare the morphology, molecular conformation, and microstructural length scales of Y-, H-, and π -shaped diblock copolymers.

In simple A_mB_n miktoarm star copolymers, Milner et al.^[2,3] applied the strong segregation theory (SST) to construct the phase diagram in terms of the composition and the asymmetric parameter $\varepsilon [= (n_A/n_B)(l_A/l_B)^{1/2}]$, where n_I and l_I are the number of arms and characteristic length of component, for $I = A, B$, respectively. The length parameter l_I is defined as $l_I = V_I/R_I^2$, where V_I and R_I correspond to the molecular volume and the radius of gyration of the respective blocks I , respectively. They reported that at the same composition, varying the asymmetric parameter ε could trigger the evolution of various microstructures. For instance, upon increasing the number of B arms in the AB_n miktoarm star copolymers, a transition towards decreasing f_A is expected. This is reasonable since the component with more arms experiences more lateral crowding and becomes more stretched, it tends to remain on the outside domains. Recently, Grason and Kamien^[4] employed the self-consistent mean-field (SCMF) theory to construct the phase diagram of AB_n in terms of f_A and χN , where χ is the Flory-Huggins interaction parameter, and N is degree of copolymerization.

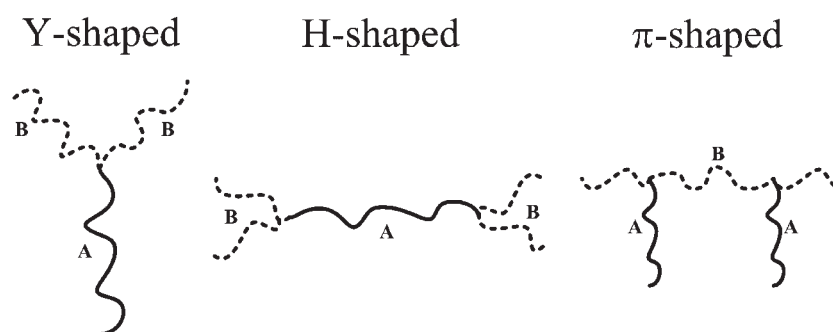
C.-I. Huang, L.-F. Yang, C.-H. Lin, H.-T. Yu
Institute of Polymer Science and Engineering, National Taiwan University, Taipei 106, Taiwan
Fax: +886 2 3366 5237; E-mail: chingih@ntu.edu.tw

Comparing with AB linear diblock copolymers, they obtained a similar phase diagram, which however slightly shifts towards $f_A > 0.5$. To clarify, the stability of microstructures with the B blocks in the majority domains is enhanced as the number of B arms n increases. Basically, these theoretical results are in good agreement with experimental results.^[5–11] However, when the composition of single arm A is large such that the SCMF theory predicts a hexagonally-packed B-formed cylindrical phase, what has been frequently observed is a worm-like micelle structure. Recently, we employed dissipative particle dynamics (DPD) to simulate the phase behavior of AB₂ miktoarm star copolymers.^[12] The phase diagram for the AB₂ molecules simulated by varying the composition and interaction parameter is in good agreement with that predicted by SCMF theory,^[4] except when the composition A is large. Our DPD results for large A composition values demonstrated that these AB₂ chains are not able to form the well ordered structure as easily as the SCMF theory has predicted, but instead only a tube-like phase. This is because when the multi-arms B remain on the concave side of the interface, curving the interface toward the B domains causes more lateral crowding and thereafter excess stretching in B. Hence, the formed microstructures become less ordered.

As to the morphological behavior of the H- and π -shaped diblock copolymers, most of the experimental results were explained and mapped onto the phase diagram of miktoarm star copolymers calculated in the strong segregation regimes by Milner. For example, Lee et al.^[13,14] synthesized a series of polystyrene (PS) and polyisoprene (PI) diblock copolymers with H- and π -architectures. They reported that the resulting phase behavior is approximately equivalent to that of the constituting Y-shaped architecture copolymers, which are the fundamental building blocks obtained by imaginarily cutting the middle of the H- and π -shaped molecules. This may hold true in the copolymers with substantially high molecular weights and/or in the strong segregation regime since the entropic penalty when two

Y-shaped molecules are joined to form an H- or π -shaped molecule is negligible. However, for the low molecular weights of materials in weak to intermediate segregation regimes, the entropic effect associated with these more complex architectures (i.e., multiple junction points) becomes more significant and cannot be neglected anymore. This definitely has an influence on the resulting morphological behavior of H- and π -shaped copolymers from weak to intermediate segregation regimes.

In this paper, we thus aim to employ DPD to compare the microphase separation behavior, and analyze the molecular conformation and structural size of Y-shaped (AB₂), H-shaped (B₂AB₂), and π -shaped [B(A)B(A)B] copolymers. Each simulated copolymer architecture is illustrated in Figure 1. Generally speaking, the DPD method simplifies a long series of molecular groups into a few bead-and-spring type particles and, therefore, it can simulate the molecular behavior on longer time-scales and larger length-scales compared with the classical molecular dynamics and Monte Carlo simulations. Groot and Madden^[22] were the first to successfully apply DPD to the microphase separation behavior of linear AB diblock copolymers. The phase diagram they constructed, though based on the results for short AB chains with the total number of beads per chain N equal to 10, is found in near quantitative agreement with that predicted by the SCMF theory,^[23] provided that the fluctuation effects caused by finite chains are included.^[24] Similarly, our recent DPD results for the AB₂ molecules with the total number of beads per chain N equal to 20 have also captured most of the experimentally observed morphological transitions. Here, in order to compare the difference among each architecture, we choose the total number of beads for a molecular chain to be fixed at $N=20$, and vary the A composition $f_A = N_A/N$, where N_A corresponds to the total number of A beads, as in our study of AB₂ miktoarm molecules. For simplicity, we assume that the constituting AB₂ molecules for these two H- and π -shaped copolymers, as well as the AB₂ miktoarm molecules, are symmetric – that is, each arm of the same block has the



■ Figure 1. Schematic plot of some typical graft copolymers, such as Y-shaped (AB₂), H-shaped (B₂AB₂), and π -shaped [B(A)B(A)B] copolymers.

same chain length. We first construct the phase diagram with respect to each architecture of copolymer in terms of the A composition f_A and the interaction parameter a_{AB} , respectively. Note that the phase diagram for Y-shaped (AB_2) copolymers has been presented in ref.^[12] We then analyze the radius of gyration (R_g) and the structural size for each copolymer.

DPD Simulation Method

In the DPD simulation, the time evolution of motion for a set of interacting particles is solved by Newton's equation. For simplicity, we assume that the masses of all particles are equal to 1. The force acting on the i th particle \vec{f}_i contains three parts: a conservative force \vec{F}_{ij}^C , a dissipative force \vec{F}_{ij}^D , and a random force \vec{F}_{ij}^R :

$$\vec{f}_i = \sum_{i \neq j} \left(\vec{F}_{ij}^C + \vec{F}_{ij}^D + \vec{F}_{ij}^R \right) \quad (1)$$

where the sum is over all other particles within a certain cut-off radius r_c . As this short-range cut-off counts only local interactions, r_c is usually set to 1 so that all lengths are measured relative to the particle radius.

The conservative force \vec{F}_{ij}^C is a soft repulsive force and given by:

$$\vec{F}_{ij}^C = \begin{cases} -a_{ij} \left(1 - \frac{r_{ij}}{r_c} \right) \vec{n}_{ij} & r_{ij} < r_c \\ 0 & r_{ij} \geq r_c \end{cases} \quad (2)$$

where a_{ij} is the repulsive interaction parameter between particles i and j , $\vec{r}_{ij} = \vec{r}_j - \vec{r}_i$, $r_{ij} = |\vec{r}_{ij}|$, and $\vec{n}_{ij} = \frac{\vec{r}_{ij}}{r_{ij}}$.

The dissipative force \vec{F}_{ij}^D is a hydrodynamic drag force and given by:

$$\vec{F}_{ij}^D = \begin{cases} -\gamma \omega^D(r_{ij}) (\vec{n}_{ij} \cdot \vec{v}_{ij}) \vec{n}_{ij} & r_{ij} < r_c \\ 0 & r_{ij} \geq r_c \end{cases} \quad (3)$$

where γ is a friction parameter, ω^D is a r -dependent weight function vanishing for $r \geq r_c$, and $\vec{v}_{ij} = \vec{v}_j - \vec{v}_i$.

The random force \vec{F}_{ij}^R corresponds to the thermal noise and has the form:

$$\vec{F}_{ij}^R = \begin{cases} \sigma \omega^R(r_{ij}) \theta_{ij} \vec{n}_{ij} & r_{ij} < r_c \\ 0 & r_{ij} \geq r_c \end{cases} \quad (4)$$

where σ is a parameter, ω^R is a weight function, and $\theta_{ij}(t)$ is a randomly fluctuating variable. Note that these two forces \vec{F}_{ij}^D and \vec{F}_{ij}^R also act along the line of centers and conserve linear and angular momentum. There is an independent random function for each pair of particles. Also there is a

relation between both constants γ and σ as follows:^[25]

$$\sigma^2 = 2\gamma k_B T \quad (5)$$

In our simulations, $\gamma = 4.5$ and the temperature $k_B T = 1$. As such, $\sigma = 3.0$ according to Equation (5).

In order for the steady-state solution to the equation of motion to be the Gibbs ensemble and for the fluctuation-dissipation theorem to be satisfied, it has been shown that only one of the two weight functions ω^D and ω^R can be chosen arbitrarily.^[26]

$$\omega^D(r) = [\omega^R(r)]^2 \quad (6)$$

which, in further, is usually taken as:

$$\omega^D(r) = [\omega^R(r)]^2 = \begin{cases} \left(1 - \frac{r_{ij}}{r_c} \right)^2 & r_{ij} < r_c \\ 0 & r_{ij} \geq r_c \end{cases} \quad (7)$$

Finally, the spring force \vec{f}^S , which acts between the connected beads in a molecule, has the form of

$$\vec{f}_i^S = \sum_j C \vec{r}_{ij} \quad (8)$$

where C is a harmonic type spring constant for the connecting pairs of beads in a molecule, and is chosen equal to 4 (in terms of $k_B T$).^[25]

Note that a modified version of the velocity-Verlet algorithm is used here to solve the Newtonian equation of motion.^[27]

$$\begin{aligned} r_i(t + \Delta t) &= r_i(t) + v_i(t) \cdot \Delta t + \frac{1}{2} f_i(t) \cdot \Delta t^2 \\ \tilde{v}_i(t + \Delta t) &= v_i(t) + \lambda f_i(t) \cdot \Delta t \\ f_i(t + \Delta t) &= f_i[r_i(t + \Delta t), \tilde{v}_i(t + \Delta t)] \\ v_i(t + \Delta t) &= v_i(t) + \frac{1}{2} \Delta t \cdot [f_i(t) + f_i(t + \Delta t)] \end{aligned} \quad (9)$$

The parameter λ is introduced to account for some additional effects of the stochastic interactions. A detailed investigation of the effects of λ on the steady state temperature has been reported by Groot and Warren.^[25] For the particle density $\rho = 3$ and the constant $\sigma = 3$, they found an optimum value of $\lambda = 0.65$, in which the temperature control can be significantly maintained even at a large time step of 0.06. Here, we choose $\lambda = 0.65$ and the time step $\Delta t = 0.05$ according to ref.^[25]

The DPD simulations are performed in a cubic box of L^3 grids with periodic boundary conditions. The particle density ρ is set equal to 3. Hence, the total simulated DPD beads are $3L^3$. On the basis of the algorithm described above, the time evolutions of motion for these particles are started with an initially disordered configuration and

simulated within the cubic box. Each simulation is performed until the formed structure remains somewhat unchanged with the time step. In general, the resulting morphology patterns via DPD are dependent on the finite size of the simulation box, as have been reported in other theoretical studies.^[28–30] In order to exclude the finite size effects, one has to keep enlarging the simulation box size until the structures are no longer affected by the simulation box. For our current model system with the total number of beads per chain $N=20$, the simulated box size is typically chosen as $15 \times 15 \times 15$ to about $20 \times 20 \times 20$, which is large enough to ensure that the finite size effects would not influence the morphological results. In each simulated morphology pattern, the dark grey and light grey colors are used to represent A and B, respectively.

Results and Discussion

In simulating the phase behavior of Y-, H-, and π -shaped copolymers by DPD, the dimensionless interaction para-

meter (i.e., in terms of $k_B T$) between like particles $a_{ii}=25$ for the particle density $\rho=3$ according to the work of Groot and Warren.^[25] The interaction parameter between different components i and j can be estimated by the relationship between a_{ij} and the Flory-Huggins interaction parameter χ_{ij} derived by Groot and Warren,^[25] for $\rho=3$, $a_{ij}(T) = a_{ij} + 3.497\chi_{ij}(T)$. Therefore, the value of $a_{ij} \leq 25$ corresponds to $\chi_{ij} \leq 0$, which indicates that components i and j are very miscible. As the incompatibility between i and j increases, a_{ij} increases from 25.

Figure 2a–c displays the phase diagrams of Y-, H-, and π -shaped diblock copolymers simulated by DPD, respectively. Note that the phase behavior of Y-shaped (AB_2) copolymers has been discussed in detail previously.^[12] Here we include it for a comparison. As in the case of linear AB diblock copolymers, these three architectures of copolymers form similar ordered structures, such as lamellae (L), gyroid (G), perforated lamellae (PL), hexagonally packed cylinders (C^{HEX}), and ordered spheres (S), which are mainly dominated by the composition f_A . However, due to the fact that the two H- and π -shaped molecules

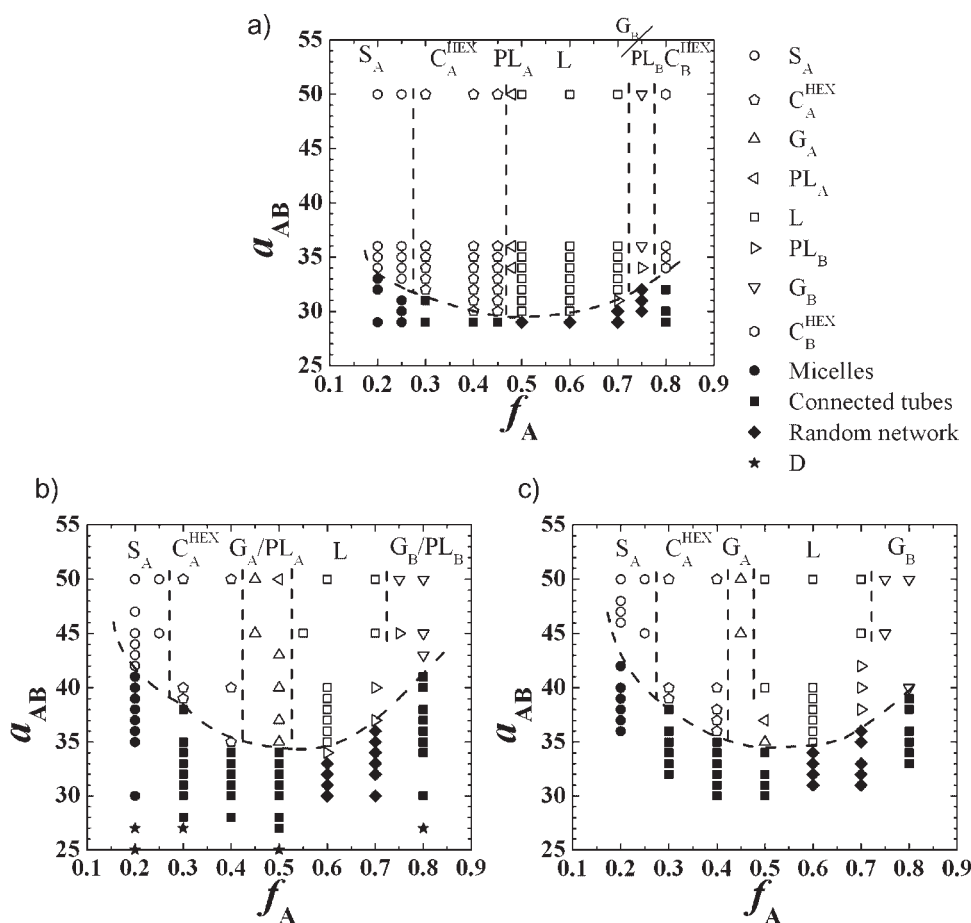


Figure 2. Phase diagram of: a) Y-shaped, b) H-shaped, and c) π -shaped molecules, in terms of the interaction parameter a_{AB} and composition f_A via DPD. The phase boundary lines are drawn as a guide for the eyes.

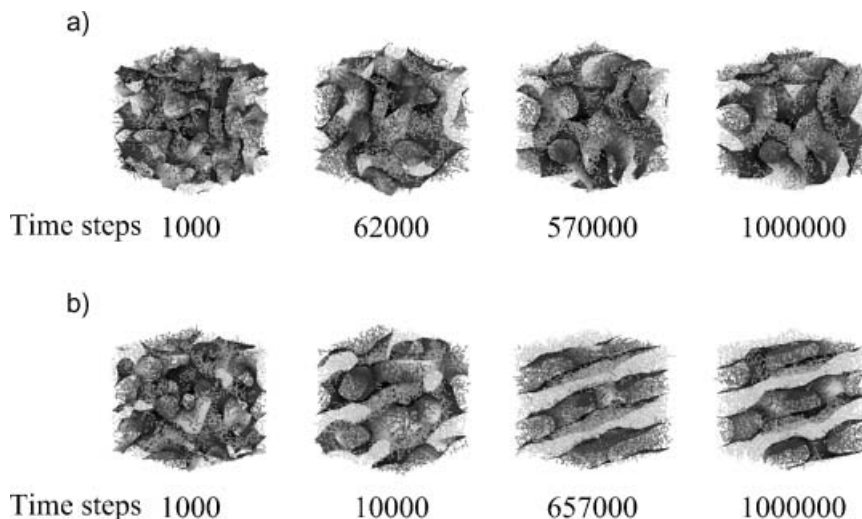


Figure 3. Time-resolved morphology patterns of H-architecture molecules with $f_A = 0.5$ and $a_{AB} =$ (a) 37 and (b) 50, respectively, simulated in a box of $15 \times 15 \times 15$. The dark grey and light grey colors represent A and B, respectively. The dark grey surface corresponds to the isosurface of component A.

have more junction points than Y-shaped, the change of entropy loss associated with the disorder-to-order transition becomes greater. Accordingly, it is more difficult for both H and π copolymers to undergo a microphase separation than for a Y copolymer, and we observe a significant increase of the order-disorder transition (ODT) value of the interaction parameter a_{AB} . Furthermore, when two Y-shaped AB_2 molecules are combined to form an H- or π -shaped molecule, it is reasonable to infer that the component with more branches (i.e., B) experiences more lateral crowding and becomes more stretched. Therefore, one may expect that the B component tends to remain on the outside domains, and the ordered regime of microstructures with the B blocks in the majority domains is significantly enlarged in both H- and π -shaped copolymers. For instance, when $f_A = 0.5$, provided that the interaction parameter a_{AB} exceeds the ODT value, the Y-shaped AB_2 copolymer forms a lamellar phase, while the H- and π -shaped copolymers can form G_A and PL_A (the A component acts like a minority component). Figure 3a and b illustrates the time-evolution of morphology patterns for H-architecture copolymer with $f_C = 0.5$ at $a_{AB} = 37$ and 50, respectively. As can be seen clearly in Figure 3a, when the interaction parameter a_{AB} is lower ($a_{AB} = 37$), the system first decomposes very quickly to form a 3D interconnected structure of A minority domains in the matrix formed by the B component, and then transforms into a G_A phase as the time step increases. When the interaction parameter a_{AB} becomes larger ($a_{AB} = 50$), due to the fact that the two A and B components would like to segregate each other to further reduce interfacial area, we observe that the initially formed interconnected A-tubes gradually get coarsened and

transform into perforated layers of A (Figure 3b). One may expect that this PL_A phase would further evolve into a lamellar phase; however, the simulated structure pattern up to 10^6 time steps still shows the formation of PL_A . Similar formation of complex phases, such as G_A and PL_A , has also been observed in π -shaped copolymer with $f_A = 0.5$ at lower values of a_{AB} ($34 < a_{AB} < 40$). If we further increase $a_{AB} \geq 40$, we find that the π copolymer with $f_A = 0.5$ can undergo a series of time-evoluted transitions from interconnected A-tubes $\rightarrow PL_A \rightarrow L$, as in Figure 4, where $a_{AB} = 50$. The fact that π copolymer can form a lamellar phase while the H copolymer still remains PL_A with increasing the interaction parameter is not surprising, since the H copolymer has more B-branch arms and, thus, needs more space to stretch out and prefer to stay in the matrix domains. A further comparison between these

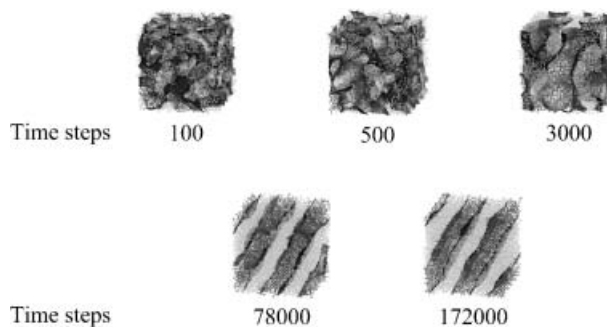


Figure 4. Time-resolved morphology patterns of π -architecture molecules with $f_A = 0.5$ and $a_{AB} = 50$, simulated in a box of $15 \times 15 \times 15$. The dark grey and light grey colors represent A and B, respectively. The dark grey surface corresponds to the isosurface of component A.

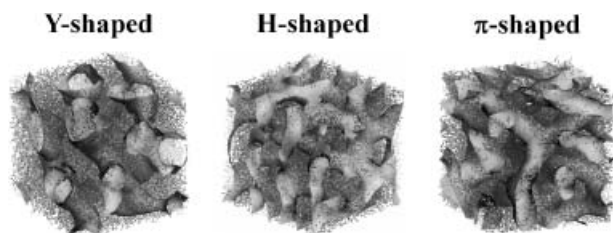


Figure 5. Morphology patterns of Y-, H-, and π - molecules when $f_A = 0.8$ and $a_{AB} = 50$, simulated in a box of $20 \times 20 \times 20$ until 10^6 time steps. The dark grey and light grey colors represent A and B, respectively. The light grey surface corresponds to the isosurface of component B.

three types of architectures can be seen more obviously in Figure 5, where we display the simulated structure patterns for f_A increasing to 0.8 and $a_{AB} = 50$. It is clear that when the component with more arms per molecule (i.e., B) is a minority, so that these B arms remain on the concave side of the interface, because curving the interface inward toward the B domains causes excess stretching of these B multi-arms, the formed microstructures become loose and less ordered. Accordingly, although the AB_2 copolymer can form a stable C_B^{HEX} phase, these B-formed cylinders still connect with each other. Moreover, both H- and π -shaped copolymers with more B arms per molecule

form a G_B phase even when B is a significantly minor component ($f_A = 0.8$).

In order to analyze the molecular conformation behavior of Y-, H-, and π -shaped molecules, we calculate the radius of gyration, R_g , for a chain, which is given as follows:

$$R_g = \left\langle R_g^2 \right\rangle^{\frac{1}{2}} = \left\langle \frac{1}{N} \sum_{i=1}^N |\vec{r}_i - \vec{r}_{\text{cm}}|^2 \right\rangle^{\frac{1}{2}} \quad (10)$$

where \vec{r}_i and \vec{r}_{cm} are the position vector of the i th bead and center of mass, respectively. Moreover, we also calculate the radius of gyration for each A and B arm by the following equations:

$$R_{g,A} = \left\langle R_{g,A}^2 \right\rangle^{\frac{1}{2}} = \left\langle \frac{1}{N'_A} \sum_{i=1}^{N'_A} |\vec{r}_{i,A} - \vec{r}_{\text{cm},A}|^2 \right\rangle^{\frac{1}{2}} \quad (11a)$$

$$R_{g,B} = \left\langle R_{g,B}^2 \right\rangle^{\frac{1}{2}} = \left\langle \frac{1}{N'_B} \sum_{i=1}^{N'_B} |\vec{r}_{i,B} - \vec{r}_{\text{cm},B}|^2 \right\rangle^{\frac{1}{2}} \quad (11b)$$

The N'_A and N'_B in Equation (11a) and (11b) represent the number of beads of one A-arm and one B-arm, respectively.

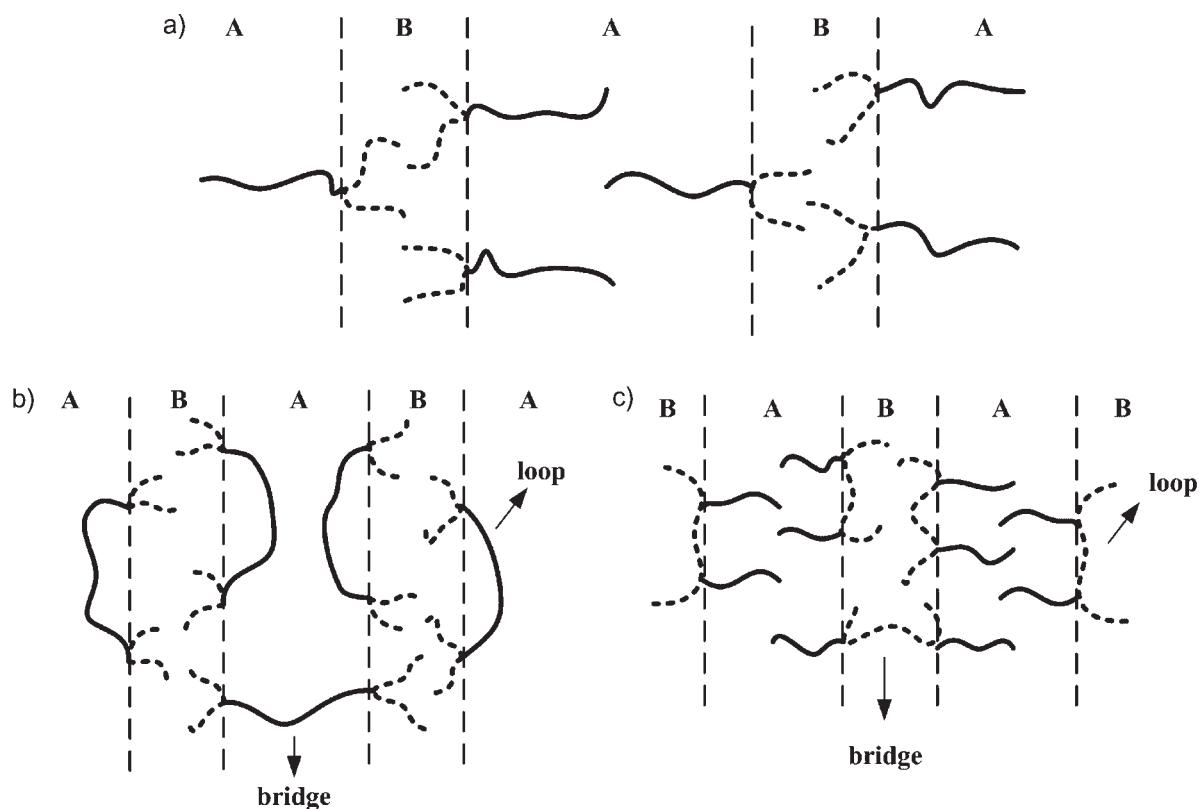


Figure 6. Schematic plot of chain conformations of: a) Y, b) H, and c) π molecules, respectively, within a lamellar structure.

Therefore, the corresponding N'_A and N'_B for Y-(AB₂), H-(B₂AB₂), and π -[B(A)B(A)B] molecule are: $N'_A = N_A$ and $N'_B = (1/2) N_B$; $N'_A = N_A$ and $N'_B = (1/4) N_B$; and, $N'_A = (1/2) N_A$ and $N'_B = N_B$, respectively.

In general, when the H- and π -shaped molecules pack to form an ordered microstructure, two types of chain conformations, loop and bridge, frequently occur within the segregated domains. Figure 6a–c illustrates the schematic chain conformations of Y-, H-, and π -molecules, respectively, within a lamellar structure. For example, in a bridge conformation for an H-molecule, both ends of the B branches reside on the different interfaces, while the two ends for an H-molecule in a loop conformation lie on the same interface. Similarly, for a π -molecule, we can also find both loop and bridge conformations, which have the two A branches located at the same interface and separate interfaces, respectively. The fractions of bridge conformation for H- and π -molecules in a lamellar structure, which are analyzed as a function of the interaction parameter a_{AB} when $f_A = 0.6$ in Figure 7, are typically in the range of 0.35–0.5. Since the molecular chains in a bridge conformation tend to stretch, while those in a loop conformation tend to curl, the resulting radius of gyration of these two conformations is significantly different. Hence, we respectively analyze the variation in R_g , $R_{g,A}$, and $R_{g,B}$ of loop and bridge conformations with the interaction parameter a_{AB} for H- and π -molecules when $f_A = 0.6$, as displayed in Figure 8a and b, respectively. For a comparison, we also include the plot of R_g , $R_{g,A}$, and $R_{g,B}$, as a function of a_{AB} for Y-molecules when $f_A = 0.6$ in Figure 8c, which has been published previously.^[12] In each plot the vertical error bars provide the dispersion of the radius of gyration, expressed as one standard deviation within around ± 10 –15%. As can

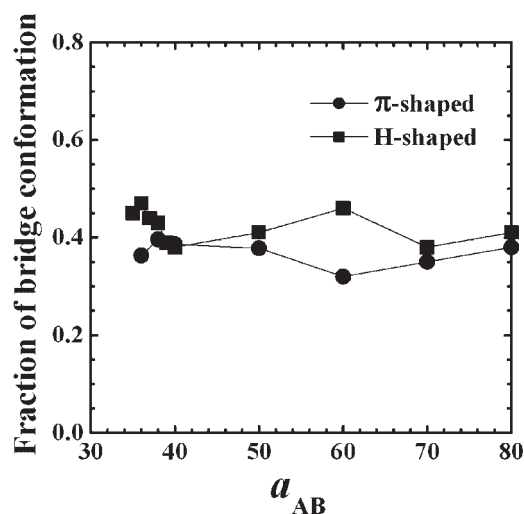


Figure 7. Fraction of H and π molecules in a bridge conformation formed, when $f_A = 0.6$, as a function of the interaction parameter a_{AB} .

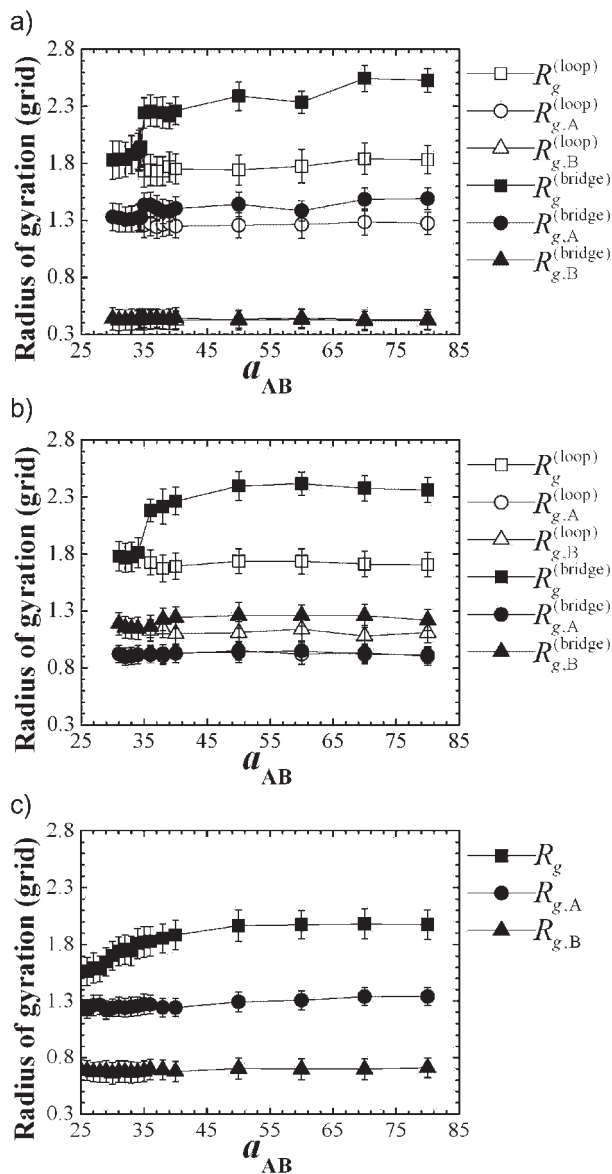


Figure 8. Plot of radius of gyration (R_g , $R_{g,A}$, $R_{g,B}$) for: a) H, b) π , and c) Y molecules, with $f_A = 0.6$ versus the interaction parameter a_{AB} .

be seen clearly in Figure 8a and b, both H-shaped and π -shaped molecules have a similar trend in that, when the system enters the ordered regime ($a_{AB} > 35$), there is a sharp increasing behavior of R_g when the molecules adopt a bridge conformation but a decreasing behavior for molecules in a loop conformation. To clarify, the molecules in a bridge conformation become more stretched than the disordered chains, whereas those in a loop conformation become more curled. With respect to the values of the radius of gyration for each A-arm and B-arm, $R_{g,A}$ and $R_{g,B}$, we observe that the R_g value of the backbone chain (i.e., the A-arm in H- and the B-arm in π -) shows the same trend with the interaction parameter a_{AB} as R_g for the whole chain; whereas the R_g value of the branch chain (i.e., the

B-arm in H and the A-arm in π) barely varies with the interaction parameter a_{AB} , even when the system transforms from the disordered into the ordered state. These results are manifested in the fact that the significant increase of the R_g value when the molecules adopt a bridge conformation is mainly attributed to the stretching of the backbone chains along the segregated lamellar domains. However, for the Y-shaped molecules (Figure 8c), though we also observe the significant increase of R_g for the whole chain when the system enters the ordered regime, the R_g values of each A and B arm remain relatively unchanged. We previously have reported that this is mainly due to the fact that in order to reduce the contacts between A and B, the unlike A and B arms tend to separate from each other, and the two B arms are squeezed onto the same side.^[12]

Basically, the above results of the molecular conformation behavior by varying the interaction parameter a_{AB} for each Y, H, and π molecular architecture when $f_A = 0.6$ also hold true qualitatively for systems with other compositions. Next, we compare the structural length scales between these three systems. Figure 9a–c shows the variation in lamellar domain spacing L , the width of the A-rich domains L_A , and the width of the B-rich regions L_B , with the changes in a_{AB} for H, π , and Y molecules, respectively, when $f_A = 0.6$. Here, we divide the lamellar domains into A-rich and B-rich domains, in which the volume fraction of A and B, respectively, is larger than 0.5. As expected, due to the increasing segregation degree between A and B with an increase in the interaction parameter a_{AB} , all the three length scales (L_A , L_B , and L) increase with a_{AB} for each system. Furthermore, we observe that the lamellae formed by Y-shaped copolymers have a significantly larger value of the domain spacing, L , than those formed by H- and π -shaped copolymers. A reasonable explanation may be given as follows: when the H- and π -shaped molecules pack to form an ordered lamellar structure, as shown schematically in Figure 6b and c, due to the significant fraction of the chains in a bridge conformation, the two A-B junction points for a bridged chain tend to locate at separate interfaces, and thus the width of the domains rich in the backbone component (i.e., A-rich for H-shaped and B-rich for π -) is restricted to approximately only one chain length. To demonstrate this, we calculate the ratio of L_A (Figure 9a) and $R_{g,A}^{(\text{bridge})}$ (Figure 8a) for H-molecules, and the ratio of L_B (Figure 9b) and $R_{g,B}^{(\text{bridge})}$ (Figure 8b) for π -molecules, which range between 2.4–2.8 and 2.0–2.2, respectively. It is clear that both ratios are very close to $\sqrt{6}$, which is typically the ratio of end-to-end distance and radius of gyration for one chain. However, for Y-shaped molecules, because of the fact that there exists only one junction point per chain, the width of the segregated domains is typically caused by two chains stretching along the lateral direction. Hence, we observe that the ratio of L (Figure 9c) and R_g (Figure 8c)

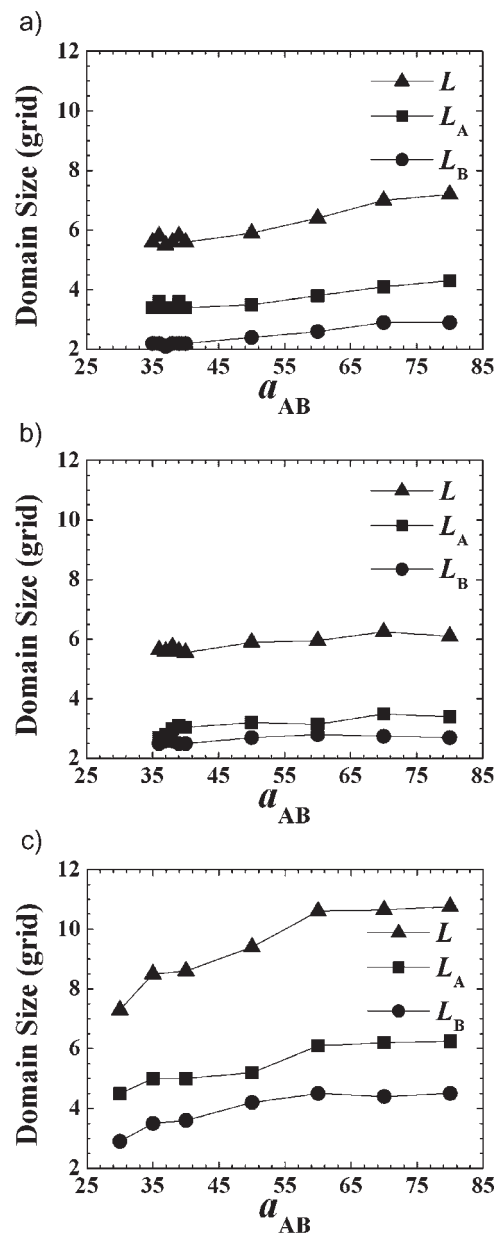

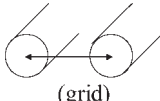



Figure 9. Plot of lamellar domain spacing L , the A-rich domain width L_A , and the B-rich domain width L_B , for: a) H, b) π , and c) Y molecules, with $f_A = 0.6$ versus the interaction parameter a_{AB} .

for Y-shape, which increases from 4.4 and reaches somewhat a constant of 5.4 with an increase in a_{AB} , does not deviate much from $2\sqrt{6}$. It should be mentioned that for other morphology types, such as cylinders and spheres, we also observe that the characteristic structural sizes in Y-shaped molecules are larger than those in H- and π -molecules, as listed in Table 1. Indeed, this is not surprising since the fact that the presence of bridges which link separate interfaces strongly limits the structural size in H and π systems, as we analyze above for lamellae, should also hold true for other microstructures.

Table 1. Characteristic length scales of cylinders and spheres formed by Y-, H-, and π -shaped molecules, respectively, at various values of composition f_A and $a_{AB} = 50$.

Composition f_A	Molecular architecture	Hexagonally Packed Cylinders		Spheres
				
0.2	Y-shaped	–	6.2	
	H-shaped	–	4.6	
	π -shaped	–	4.8	
0.25	Y-shaped	–	6.5	
	H-shaped	–	5.1	
	π -shaped	–	5.0	
0.4	Y-shaped	6.8	10.2	–
	H-shaped	5.2	8.0	–
	π -shaped	5.3	7.7	–

Finally, we would like to point out that the current bead-and-spring model in the DPD simulations allows bond crossing, and hence cannot capture the entanglement phenomenon of long polymer chains. One may question whether our current results will be affected by correcting this non-physical bond crossing behavior. In order to examine this, we modify the DPD simulation method by enhancing the spring-spring repulsion to reduce the frequency of chain segment crossing, as in the work of Pan and Manke.^[31] The segmental repulsion force has the same form as the conservative force \vec{F}_{ij}^C in Equation (2). By avoiding the bond crossing frequency, we set the new cut-off radius $r'_c = 1/2$ and the new repulsive interaction parameter, a'_{ij} , to be twice the original a_{ij} . We specifically compare the original parameters of $a_{AA} = a_{BB} = 25$, $a_{AB} = 50$, $r_c = 1$, to the new parameters of $a'_{AA} = a'_{BB} = 50$, $a'_{AB} = 50$, $r'_c = 1/2$ for Y-, H-, and π -shaped copolymers when $f_A = 0.5$ and 0.6 . We find that the bond crossing correction has little effect on the resulting equilibrium phase behavior as well as the structural size although it takes longer for the molecules to reach the equilibrium morphology. Accordingly, our current morphological results of comparing Y-, H-, and π -shaped copolymers, which are mainly based on the soft bead-and-spring DPD model, should also hold true for the molecules in the entangled regime.

Conclusion

We employ dissipative particle dynamics (DPD) to compare the phase behavior, molecular conformation behavior, and microstructural length scales of Y-shaped

(AB_2), H-shaped (B_2AB_2), and π -shaped $[B(A)B(A)B]$ copolymers. Similar to linear diblock copolymers, these three molecular architectures of copolymers can form various types of ordered structures, such as lamellae, gyroid, perforated lamellae, hexagonally packed cylinders, and ordered spheres, which are mainly dominated by the composition. However, with increasing the complexity of molecular architecture (linear \rightarrow Y \rightarrow H or π), the phase diagram, which is constructed in terms of the interaction parameter and composition f_A , shifts more towards $f_A > 0.5$. Our results are manifested in the fact that the resulting phase diagrams of H- and π -shaped copolymers can not be mapped onto the phase diagram of miktoarm star copolymers from weak to intermediate segregation regimes. In particular, the most significant deviations are mainly the following two points: First, when the component with more arms per molecule (i.e., B) is a significantly minor, both H- and π -shaped copolymers tend to form a complex gyroid or perforated lamellar phase instead of the hexagonally packed B-formed cylinders for Y-shaped copolymers; Second, since H- and π -shaped molecules have more junction points than Y-shaped, the change of entropy loss associated with the disorder-to-order transition becomes larger. Accordingly, we observe a significant increase of the order-disorder transition value of the interaction parameter.

In analyzing the molecular conformation behavior and the microstructural length scales, we find that, due to the presence of the H and π chains in a bridge conformation in which the two A-B junction points tend to locate at separate interfaces, the resulting microstructural length scales in H and π systems are significantly smaller than those in Y-shaped molecules.

Acknowledgements: This work was supported by the *National Science Council of the Republic of China* through grant NSC 96-2221-E-002-019.

Received: November 7, 2007 Revised: January 31, 2008; Accepted: January 31, 2008; DOI: 10.1002/mats.200700068

Keywords: block copolymers; dissipative particle dynamics; molecular architecture

- [1] M. Olvera de la Cruz, I. C. Sanchez, *Macromolecules* **1986**, *19*, 2501.
- [2] S. T. Milner, *Macromolecules* **1994**, *27*, 2333.
- [3] P. D. Olmsted, S. T. Milner, *Macromolecules* **1998**, *31*, 4011.
- [4] G. M. Grason, R. D. Kamien, *Macromolecules* **2004**, *37*, 7371.
- [5] D. J. Pochan, S. P. Gido, S. Pispas, J. W. Mays, A. J. Ryan, J. P. A. Fairclough, I. W. Hamley, N. J. Terrill, *Macromolecules* **1996**, *29*, 5091.
- [6] G. Floudas, S. Pispas, N. Hadjichristidis, T. Pakula, I. Erukhimovich, *Macromolecules* **1996**, *29*, 4142.
- [7] Y. Tselikas, H. Iatrou, N. Hadjichristidis, K. S. Liang, K. Mohanty, D. J. Lohse, *J. Chem. Phys.* **1996**, *105*, 2456.
- [8] C. Lee, P. Gido, M. Pitsikalis, J. W. Mays, N. B. Tan, S. F. Trevino, N. Hadjichristidis, *Macromolecules* **1997**, *30*, 3732.
- [9] N. Hadjichristidis, *J. Polym. Sci., Part A: Polym. Chem.* **1999**, *37*, 857.
- [10] L. Yang, S. Hong, S. P. Gido, G. Velis, N. Hadjichristidis, *Macromolecules* **2001**, *34*, 9069.
- [11] A. Mavroudis, A. Avgeropoulos, N. Hadjichristidis, E. L. Thomas, D. J. Lohse, *Chem. Mater.* **2003**, *15*, 1976.
- [12] C. I. Huang, H. T. Yu, *Polymer* **2007**, *48*, 4537.
- [13] C. Lee, S. P. Gido, Y. Poulos, N. Hadjichristidis, N. B. Tan, S. F. Trevino, J. W. Mays, *J. Chem. Phys.* **1997**, *107*, 6460.
- [14] C. Lee, S. P. Gido, Y. Poulos, N. Hadjichristidis, N. B. Tan, S. F. Trevino, J. W. Mays, *Polymer* **1998**, *39*, 4631.
- [15] Y. G. Li, P. J. Shi, C. Y. Pan, *Polymer* **2004**, *37*, 5190.
- [16] D. H. Han, C. Y. Pan, *J. Polym. Sci., Part A: Polym. Chem.* **2006**, *44*, 2794.
- [17] J. Liu, C. Y. Pan, *Polymer* **2005**, *46*, 11133.
- [18] J. Xu, Z. S. Ge, Z. Y. Zhu, S. Z. Luo, H. W. Liu, S. Y. Liu, *Macromolecules* **2006**, *39*, 8178.
- [19] X. F. Yu, T. F. Shi, Z. Guo, L. J. An, *Polymer* **2006**, *47*, 1538.
- [20] D. H. Han, C. Y. Pan, *Eur. Polym. J.* **2006**, *42*, 507.
- [21] S. P. Gido, C. Lee, D. J. Pochan, S. Pispas, J. W. Mays, N. Hadjichristidis, *Macromolecules* **1996**, *29*, 7022.
- [22] R. D. Groot, T. J. Madden, *J. Chem. Phys.* **1998**, *108*, 8713.
- [23] M. W. Matsen, F. S. Bates, *Macromolecules* **1996**, *29*, 1091.
- [24] G. H. Fredrickson, E. Helfand, *J. Chem. Phys.* **1987**, *87*, 697.
- [25] R. D. Groot, P. B. Warren, *J. Chem. Phys.* **1997**, *107*, 4423.
- [26] P. Espanol, P. B. Warren, *Europhys. Lett.* **1995**, *30*, 191.
- [27] M. P. Allen, D. J. Tildesley, "Computer Simulation of Liquids", Clarendon, Oxford 1987.
- [28] U. Micka, K. Binder, *Macromol. Theory Simul.* **1995**, *4*, 419.
- [29] Y. Bahbot-Raviv, Z. G. Wang, *Phys. Rev. Lett.* **2000**, *85*, 3428.
- [30] Q. Wang, P. F. Nealey, J. J. de Pablo, *Macromolecules* **2001**, *34*, 3458.
- [31] G. Pan, C. W. Manke, *Int. J. Mod. Phys. B* **2003**, *17*, 231.